IVYSPRING INTERNATIONAL PUBLISHER

Theranostics

2018; 8(5): 1340-1349. doi: 10.7150/thno.22806

Research Paper

Desmin- and vimentin-mediated hepatic stellate cell-targeting radiotracer ^{99m}Tc-GlcNAc-PEI for liver fibrosis imaging with SPECT

Deliang Zhang[1], Rongqiang Zhuang[1], Zhide Guo[1], Mengna Gao[1], Lumei Huang[1], Linyi You[1], Pu Zhang[1], Jindian Li[1], Xinhui Su[2], Hua Wu[3], Xiaoyuan Chen[4] and Xianzhong Zhang[1,✉]

1. State Key Laboratory of Molecular Vaccinology and Molecular Diagnostics & Center for Molecular Imaging and Translational Medicine, School of Public Health, Xiamen University, Xiamen 361102, China.
2. Department of Nuclear Medicine, Zhongshan Hospital affiliated to Xiamen University, Xiamen 361004, Fujian, China.
3. Department of Nuclear Medicine, The First Affiliated Hospital of Xiamen University, Xiamen 361003, China.
4. Laboratory of Molecular Imaging and Nanomedicine, National Institute of Biomedical Imaging and Bioengineering, National Institutes of Health, Bethesda, Maryland, 20892 USA.

✉ Corresponding author: Xianzhong Zhang, Professor, PhD, School of Public Health, Xiamen University, Xiang'an South Rd., Xiang'an district, Xiamen 361102, China. Phone/Fax: +86(592)2880645; E-mail: zhangxzh@xmu.edu.cn.

Received: 2017.09.12; Accepted: 2017.12.08; Published: 2018.02.02

Abstract

Extracellular matrix (ECM) accumulation in liver fibrosis is caused by the activation of hepatic stellate cells (HSCs). The goal of this study was to develop a ^{99m}Tc-labeled N-acetylglucosamine (GlcNAc) that specifically interacts with desmin and vimentin expressed on activated HSCs to monitor the progression and prognosis of liver fibrosis using single-photon emission computed tomography (SPECT) imaging.

Methods: GlcNAc-conjugated polyethylenimine (PEI) was first prepared and radiolabeled with ^{99m}Tc. Noninvasive SPECT imaging with ^{99m}Tc-GlcNAc-PEI was used to assess liver fibrosis in a carbon tetrachloride (CCl_4) mouse model. The liver uptake value (LUV) of ^{99m}Tc-GlcNAc-PEI was measured by drawing the region of interest (ROI) of the whole liver as previously suggested. The LUV of the CCl_4 groups was compared with that of the olive oil group. Next, we estimated the correlation between the results of SPECT imaging and physiological indexes. After treatment with clodronate liposome, the LUV of ^{99m}Tc-GlcNAc-PEI in fibrotic mice was compared with that in control mice.

Results: ^{99m}Tc-GlcNAc-PEI is a hydrophilic compound with high radiochemical purity (>98%) and good stability. It could specifically target desmin and vimentin on the surface of activated HSCs with high affinity (the K_d values were 53.75 ± 9.50 nM and 20.98 ± 3.56 nM, respectively). The LUV of ^{99m}Tc-GlcNAc-PEI was significantly different between the CCl_4 and control groups as early as 4 weeks of CCl_4 administration (3.30 ± 0.160 vs 2.34 ± 0.114%/cc; $P < 0.05$). There was a strong correlation between the LUV and Sirius Red quantification ($R = 0.92$, $P < 0.001$). Compared with control, clodronate liposome treatment reduced the LUV of ^{99m}Tc-GlcNAc-PEI (4.62 ± 0.352 vs 2.133 ± 0.414%/cc; $P < 0.05$).

Conclusion: ^{99m}Tc-GlcNAc-PEI SPECT/CT was useful in assessing liver fibrosis and monitoring the treatment response.

Key words: hepatic fibrosis, desmin, vimentin, SPECT imaging, hepatic stellate cells, ^{99m}Tc-GlcNAc-PEI

Introduction

Liver fibrosis is the result of repeated damage to the liver in conjunction with sustained accumulation of extracellular matrix (ECM) proteins[1]. The accumulation of ECM proteins substitutes the necrotic tissue with a fibrous scar, which distorts the hepatic architecture and produces liver dysfunction[2]. The activation and proliferation of HSCs play a major role in the pathogenesis of hepatic fibrosis[3]. Activated HSCs are characterized by an accelerated rate of proliferation, excessive expression of α smooth

muscle actin (α-SMA), sustained syntheses of ECM proteins, and secretion of chemokines and fibrogenic factors[2, 4, 5]. Therefore, the imaging of activated HSCs may be a good strategy to assess liver fibrosis.

The accurate staging of liver fibrosis in chronic liver diseases is crucial for the prognostic assessment of the disease course and selection of feasible therapies. To this day, liver biopsy remains the gold standard for the assessment of liver fibrosis[6,7]. However, liver biopsy is an invasive procedure, and there are complications such as bleeding and pain[5]. There is an urgent need to develop non-invasive ways to assess liver fibrosis in chronic liver disease and monitor fibrosis progression and the treatment response. Many noninvasive methods have been developed in the past decades to assess liver fibrosis, such as MRI imaging of fibrosis in two rodent models with a collagen-specific probe[8] and transient elastography of liver fibrosis by measurement of the rigidity of the liver[9], and several other methods based on potential serum markers[10]. Unfortunately, conventional imaging is less accurate in detecting mild fibrosis than that of advanced fibrosis and cirrhosis[11,12].

Recently, polymers bearing N-acetylglucosamine (GlcNAc) have been reported with a strong avidity for desmin and vimentin by binding to the rod II domain of the protein on cell surfaces[13,14]. During HSC activation, the expression of desmin and vimentin is strongly upregulated[15], and activated HSCs express more desmin and vimentin protein than quiescent HSCs and other non-parenchymal cells in the liver[16], especially in advanced fibrosis[15,17]. Kim et al.[18] reported that fluorescence imaging using an IVIS® Lumina imaging system and a GlcNAc-PEI-ICG/TGFβ1 siRNA complex could assess and treat liver fibrosis. However, a long time is needed for the accumulation of the fluorescence signal in the liver, and quick extinction of its fluorescence signal has restricted its use in clinical settings. Combined SPECT/CT imaging provides accurate anatomic data on CT, as well as functional information on SPECT images, facilitating the accurate staging of liver fibrosis[19]. Therefore, we developed a small molecular radiotracer ^{99m}Tc-GlcNAc-PEI using GlcNAc as the HSC target group incorporating PEI-1800 as the functionalized group for ^{99m}Tc labeling. The purpose of this study was to assess the potential usefulness of ^{99m}Tc-GlcNAc-PEI for SPECT/CT monitoring of the progression and prognosis of liver fibrosis in a mouse model.

Results

Characterization of GlcNAc-PEI

GlcNAc-PEI was synthesized with chitobiose and PEI-1800 (shown in Fig. 1) and was characterized by ^{1}H NMR (Fig. S1A-B) and MODI-TOF-MS (Fig. S1C). The molecular weight of GlcNAc-PEI calculated by MODI-TOF-MS was approximately 3.3 kDa. The sugar content in GlcNAc-PEI was measured by the phenol-vitriol method. After the standard curve of GlcNAc was plotted (Fig. S1D), the mass percent of sugar in GlcNAc-PEI was calculated as 42.3%.

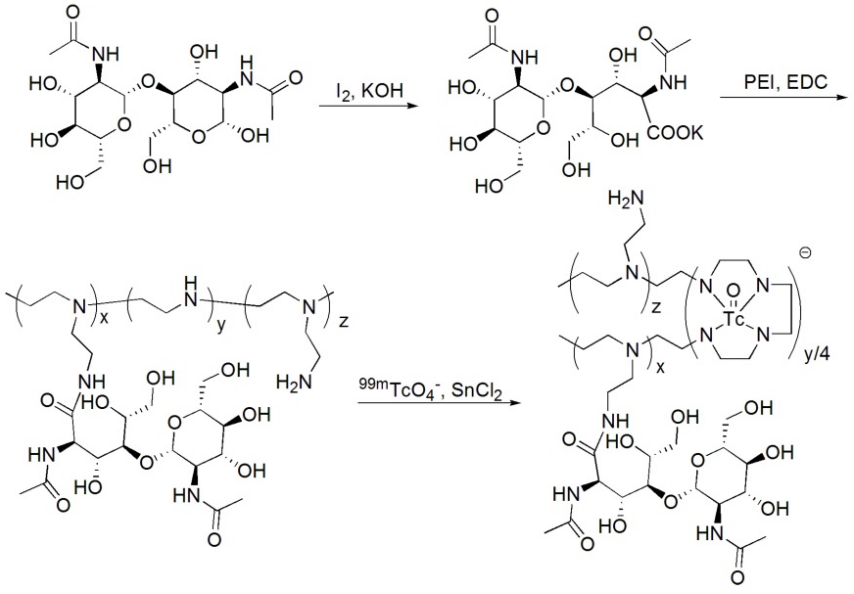

Fig. 1. Synthesis and radiolabeling of GlcNAc-PEI with ^{99m}Tc.

Radiolabeling of ^{99m}Tc-GlcNAc-PEI

The labeling efficiency of ^{99m}Tc-GlcNAc-PEI was greater than 95% as determined by TLC. ^{99m}Tc-GlcNAc-PEI remained at the spotting point (R_f = 0–0.1), while other radioactive impurities such as hydrolyzed ^{99m}Tc and $^{99m}TcO_4^-$ moved to the front of the strips (R_f = 0.9–1.0, shown in Fig. S2A). ^{99m}Tc-GlcNAc-PEI was obtained with high radiochemical purity (RCP) without purification. The RCP of ^{99m}Tc-GlcNAc-PEI was still greater than 92% when incubated in PBS or serum for 4 h, as determined by TLC (shown in Fig. S2B). The lipid-water partition coefficient of ^{99m}Tc-GlcNAc-PEI was determined by the shake flask method following the previous method, and the log P value was calculated as -3.15± 0.27 (n = 3), indicating that it was a hydrophilic compound.

Characterization of the liver fibrosis mouse model

To identify whether ^{99m}Tc-GlcNAc-PEI SPECT imaging could be used to assess liver fibrosis, we treated mice with CCl_4 or olive oil (as vehicle control) for 4 or 8 weeks to induce varying stages of liver fibrosis. Liver fibrosis gradually progressed with time and gradually developed into progressive hepatic fibrosis after the administration of CCl_4 for 8 weeks, as was expected and verified by Sirius Red staining (Fig. 2A-B). After 4 weeks of CCl_4 administration, most mice had liver injury with short fibrous septa (control vs 4 W = 1.04% ± 0.12% vs 2.26% ± 0.15%, $P < 0.05$). In the livers of CCl_4-8 W mice, extensive bridging fibrosis, in addition to distortion of the liver architecture with pseudo-lobule formation, was visible (control vs 8 W = 1.04% ± 0.12% vs 3.24% ± 0.28%, $P < 0.01$). Consistently, we detected the collagen of liver tissue by hydroxyproline analysis, and collagen deposition was increased along with the administration of CCl_4 (Fig. 2C). The Ishak score was also increased along with the administration of CCl_4 (Fig. 2D). There were strong correlations between the hydroxyproline level and Sirius Red quantification (R = 0.88, Fig. 2E), Sirius Red quantification and the Ishak score (R = 0.93, Fig. 2F), and the hydroxyproline level and Ishak score (R = 0.89, Fig. 2G). ^{18}F-FDG PET/CT imaging and ^{99m}Tc-GSA SPECT/CT imaging confirmed the pathologic process of fibrosis in the CCl_4 mice (Fig. S3).

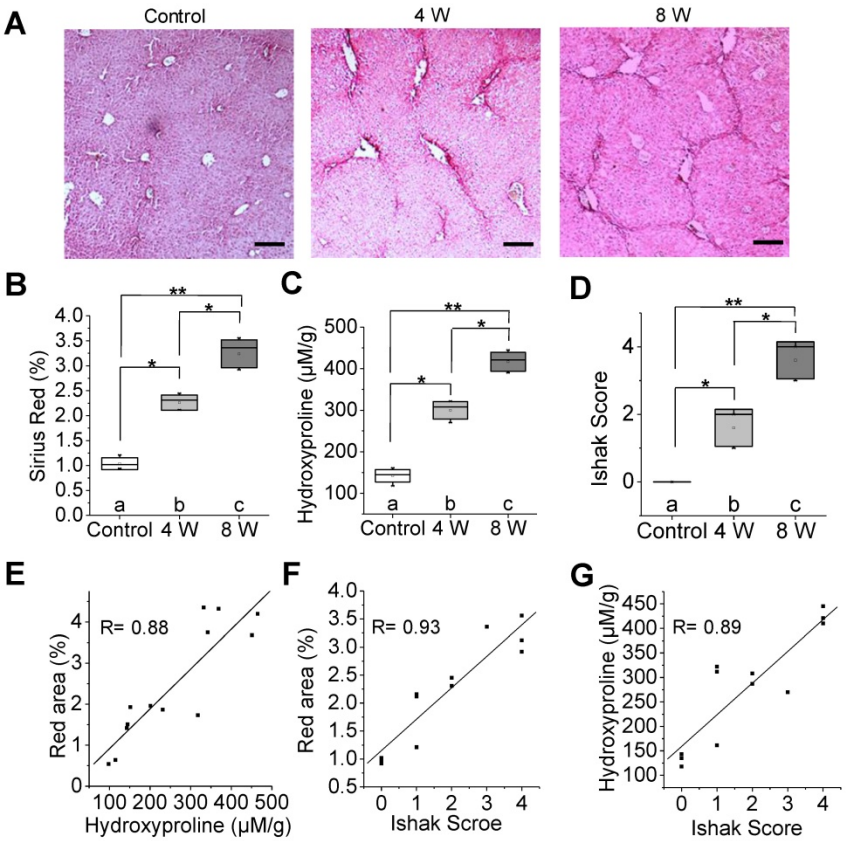

Fig. 2. Characterization of a CCl_4-induced mouse model of liver fibrosis. (A) Representative images of Sirius Red staining after CCl_4 administration for 4 or 8 weeks. Scale bar: 200 μm. (B) Red area of Sirius Red staining was quantified using Image pro-pus software. (C) Hydroxyproline level in the liver of CCl_4-induced mice was calculated by HPLC analysis. (D) Ishak score of the liver tissue in CCl_4-induced fibrotic mice. (E) Correlation between total collagen (hydroxyproline) and red area of Sirius Red staining. (F) Correlation between the total Ishak score and red area of Sirius Red staining. (G) Correlation between the Ishak score and total collagen (hydroxyproline). $^*P$ <0.05 and $^{**}P$ <0.01.

^{99m}Tc-GlcNAc-PEI SPECT imaging to assess liver fibrosis in the mice

The time-activity curves and representative images derived from the 50-min dynamic SPECT imaging (Fig. S4) showed that the hepatic uptake of fibrotic mice was higher than that of control mice and peaked within 25~30 min after injection. Thus, the static microSPECT scans were performed in control and CCl_4 mice at 30 min after injection. Strong contrast between the liver and non-targeted tissues or organs were obtained after ^{99m}Tc-GlcNAc-PEI injection. ^{99m}Tc-GlcNAc-PEI showed specific and high uptake in the liver of fibrotic mice, except for unexpected high splenic uptake and metabolites in the bladder. The hepatic uptake increased with disease progression in the CCl_4-induced fibrotic mice, as seen in Fig. 3A. The LUV of the CCl_4-8 W group was higher than that of CCl_4-4 W group (4.68 ± 0.11%/cc vs 3.30 ± 0.16%/cc, $P < 0.01$) and much higher than that of the control group (4.68 ± 0.11%/cc vs 2.34 ± 0.11%/cc, $P < 0.001$), as shown in Fig. 3B. We obtained a similar result with autoradiography of the liver tissue of the control and fibrotic mice (Fig. S5). ^{99m}Tc-GlcNAc-PEI was more likely to combine with fibrotic liver tissues than with normal liver tissues. Similar results were obtained from the biodistribution experiment (Fig. 3C). The liver uptake of ^{99m}Tc-GlcNAc-PEI in fibrotic mice was different from that in control mice (control vs 4 W = 2.54 ± 0.40%ID/g vs 4.90 ± 0.58%ID/g, $P < 0.05$; control vs 8 W = 2.54 ± 0.40%ID/g vs 7.74 ± 0.76%ID/g, $P < 0.01$). Strong correlations were observed between hepatic uptake measured by SPECT/CT and Sirius Red quantification (R = 0.92, Fig. 3D) and between hepatic uptake and the liver hydroxyproline levels (R = 0.95, Fig. 3E). Immunofluorescent assay showed strong colocalization of anti-desmin (Fig. 3F) and anti-vimentin (Fig. S6) staining (FITC) with Cy5.5-labeled GlcNAc-PEI (GlcNAc-PEI-Cy5.5), confirming that GlcNAc-PEI could target desmin and vimentin on the surface of activated HSCs. However, the liver tissue of the control group lacked the expression of desmin and vimentin and showed less binding of GlcNAc-PEI-Cy5.5. We obtained a similar result using an immunofluorescent colocalization assay with GlcNAc-PEI-Cy5.5 and anti-α-SMA staining (Fig. S7). Biodistribution experiments using ^{99m}Tc-GlcNAc-PEI in normal mice showed low uptake in the liver and extensive uptake in the spleen (Fig. S8). Next, we labeled untargeted PEI-1800 with ^{99m}Tc using the same method as ^{99m}Tc-GlcNAc-PEI for comparison. SPECT imaging of CCl_4-induced fibrotic mice with ^{99m}Tc-PEI-1800 showed high accumulation in the kidney and low splenic uptake (Fig. S9), a finding that was different from that with ^{99m}Tc-GlcNAc-PEI.

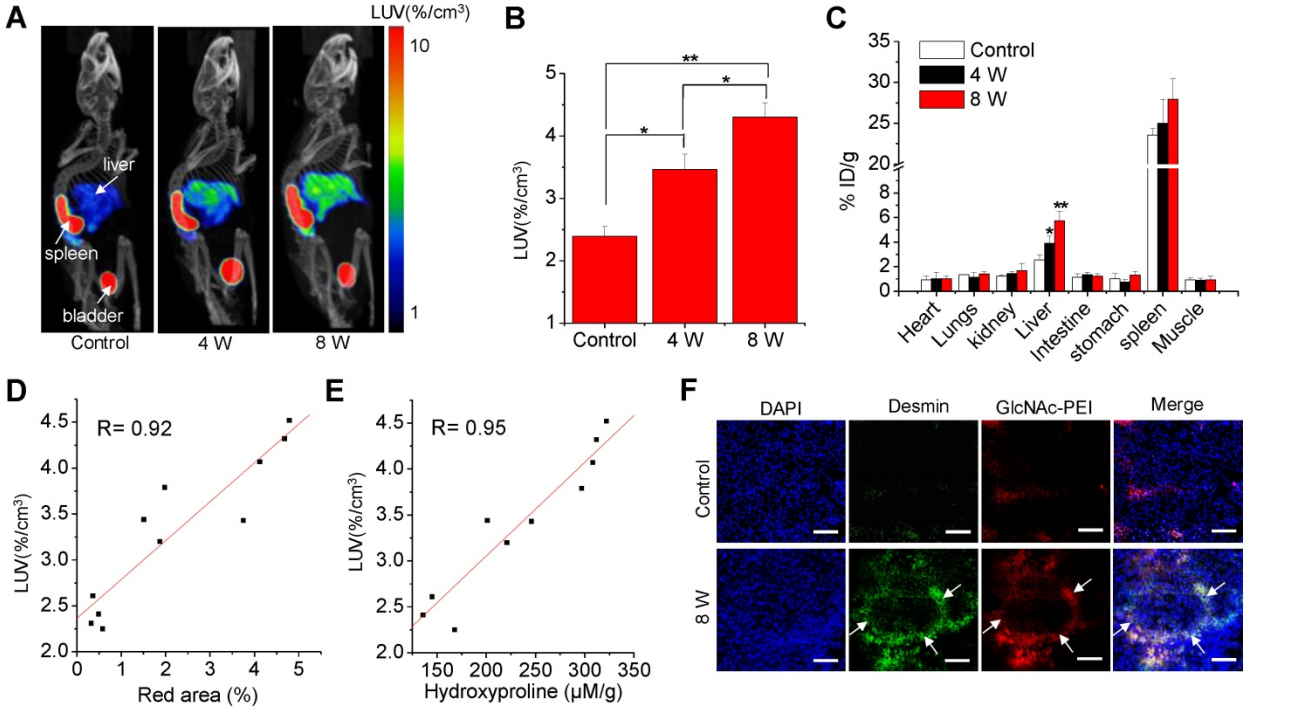

Fig. 3. MicroSPECT/CT imaging with ^{99m}Tc-GlcNAc-PEI to assess liver fibrosis. (A) SPECT/CT imaging of CCl_4-induced fibrotic mice with ^{99m}Tc-GlcNAc-PEI. Both images were rendered at the same scale. (B) Hepatic uptake of control and fibrotic mice by drawing the ROI of the whole liver. (C) Biodistribution of ^{99m}Tc-GlcNAc-PEI in CCl_4-induced fibrotic mice (n = 3). (D) Correlation between hepatic uptake and Sirius Red quantification. (E) Correlation between hepatic uptake and total collagen (hydroxyproline). (F) Immunofluorescence co-localization analysis of desmin and GlcNAc-PEI-Cy5.5 in the liver tissue of CCl_4-induced fibrotic mice. Scale bar: 200 μm. $^*P$ <0.05 and $^{**}P$ <0.01.

Blocking studies of ^{99m}Tc-GlcNAc-PEI in fibrotic mice

To confirm the desmin and vimentin specificity of ^{99m}Tc-GlcNAc-PEI in the fibrotic liver, blocking experiments were performed. After the co-injection of an excess dose of GlcNAc-PEI (500 μg), hepatic uptake was significantly reduced in fibrotic mice ($P < 0.01$; Fig. 4A, C). By contrast, co-injection of an excess dose of GlcNAc-PEI had no effect on the hepatic uptake of ^{99m}Tc-GlcNAc-PEI in the liver of normal mice. Fluorescent cell uptake of GlcNAc-PEI-Cy5.5 was decreased obviously when blocked with excess GlcNAc-PEI in HSCs isolated from the liver of fibrotic mice (Fig. 4B). The radioactive competitive binding assay indicated that cellular uptake of ^{99m}Tc-GlcNAc-PEI was significantly decreased when blocking with excess GlcNAc-PEI in the HSCs of fibrotic mice (Fig. 4D). To further assess the binding affinity, saturation binding experiments were performed with ^{99m}Tc-GlcNAc-PEI and ^{99m}Tc-PEI-1800. We found that ^{99m}Tc-GlcNAc-PEI had a classical saturation curve and a high affinity with desmin protein (K_d = 53.75 ± 9.50 nM; as shown in Fig. 4E). However, ^{99m}Tc-PEI-1800 had a nearly linear distribution similar to non-specific uptake, indicating the low affinity of ^{99m}Tc-PEI-1800. Meanwhile, we found that ^{99m}Tc-GlcNAc-PEI had a high affinity with vimentin protein (K_d = 20.98 ± 3.56 nM; as shown in Fig. S10). Through these analyses, we demonstrated that GlcNAc-PEI could specifically target desmin and vimentin on the surface of activated HSCs.

SPECT/CT imaging of liver fibrosis mice with clodronate liposome treatment

The lack of non-invasive ways to monitor fibrosis progression limited the development of anti-fibrotic drugs[20]. Here, we developed a method based on SPECT imaging with ^{99m}Tc-GlcNAc-PEI to monitor the therapeutic efficacy of liver fibrosis. Clodronate liposomes were used for the treatment of liver fibrosis because it could reduce fibrosis by killing macrophages in the liver. As seen in Fig. 5A-B, the LUV of ^{99m}Tc-GlcNAc-PEI was obviously decreased in fibrotic mice treated with clodronate liposomes (control vs clodronate = 4.62 ± 0.35%/cc vs 2.13 ± 0.41%/cc; $P < 0.05$). ^{99m}Tc-GlcNAc-PEI SPECT/CT static imaging could detect the difference between these two groups of mice in the evaluation of liver fibrosis. Histologic analysis of the Sirius Red staining results demonstrated that the collagen fiber was reduced evidently in fibrotic mice after clodronate liposome treatment (Fig. 5C). After clodronate liposome treatment, the fibrous area of most mice was reduced (control vs clodronate = 3.09 ± 0.20% vs 1.75 ± 0.19%, $P < 0.05$; Fig. 5D). Consistently, collagen deposition was decreased with the administration of clodronate (control vs clodronate = 362.8 ± 59.04 vs 158.3 ± 48.68 μmol/g; $P < 0.05$; Fig. 5E). Immunohistology studies showed that the expression of CD_{68} (cell surface marker of macrophage) was obviously decreased in the liver of fibrotic mice when treated with clodronate liposomes (Fig. 5F). Immunofluorescence analysis showed that the expression of α-SMA was significantly reduced in the liver of fibrotic mice after clodronate liposome treatment (Fig. S11). These results suggested that ^{99m}Tc-GlcNAc-PEI SPECT/CT imaging could be used as a potent method to monitor fibrosis progression and evaluate the effect of anti-fibrotic drugs.

Discussion

Previously, significantly increased expression of desmin and vimentin was reported in the fibrotic liver of mice, especially in advanced fibrosis[15,17]. In this study, we developed an HSC-targeting radiotracer, ^{99m}Tc-GlcNAc-PEI. High-quality images of the whole liver were obtained using ^{99m}Tc-GlcNAc-PEI by SPECT/CT imaging in CCl_4-induced fibrotic mice. We demonstrated that SPECT/CT imaging with ^{99m}Tc-GlcNAc-PEI could reliably identify liver fibrosis as early as 4 weeks after CCl_4 treatment. The pathologic process of fibrosis and significantly enhanced desmin and vimentin expression during the progression of liver fibrosis were verified and confirmed by histologic staining in this study. Furthermore, ^{18}F-FDG PET/CT and ^{99m}Tc-GSA SPECT/CT imaging were performed to confirm the pathologic process in the CCl_4-induced fibrotic mice. Unlike ^{99m}Tc-GlcNAc-PEI, the increased uptake of ^{18}F-FDG (Fig. S3A) and decreased uptake of ^{99m}Tc-GSA (Fig. S3C) in the fibrotic liver were caused by inflammation and hepatic injury, respectively. Both changes in radioactivity accumulation in the liver do not reflect the degree of fibrosis directly and therefore cannot be used for liver fibrosis diagnosis.

The labeling of ^{99m}Tc-GlcNAc-PEI is simple and quick. GlcNAc-PEI was successfully radiolabeled with ^{99m}Tc using the multi-amino structure of PEI at room temperature with a high radiolabeling efficiency and radiochemical stability. All the advantages of ^{99m}Tc-GlcNAc-PEI might be beneficial for it to be used in the clinic. Since PEI is a good siRNA delivery system, GlcNAc-PEI/siRNA could be used to effectively treat liver fibrosis by targeting HSCs[19]. Using the competitive binding assay and blocking SPECT imaging, we clearly demonstrated that ^{99m}Tc-GlcNAc-PEI could specifically target HSCs, leading to their activation in fibrotic mice. Immunohistology studies of the liver tissue of fibrotic

mice showed that GlcNAc-PEI could co-localize with desmin and α-SMA. Using the saturation binding assay, we found that ^{99m}Tc-GlcNAc-PEI had a much higher desmin-binding affinity than untargeted ^{99m}Tc-PEI-1800.

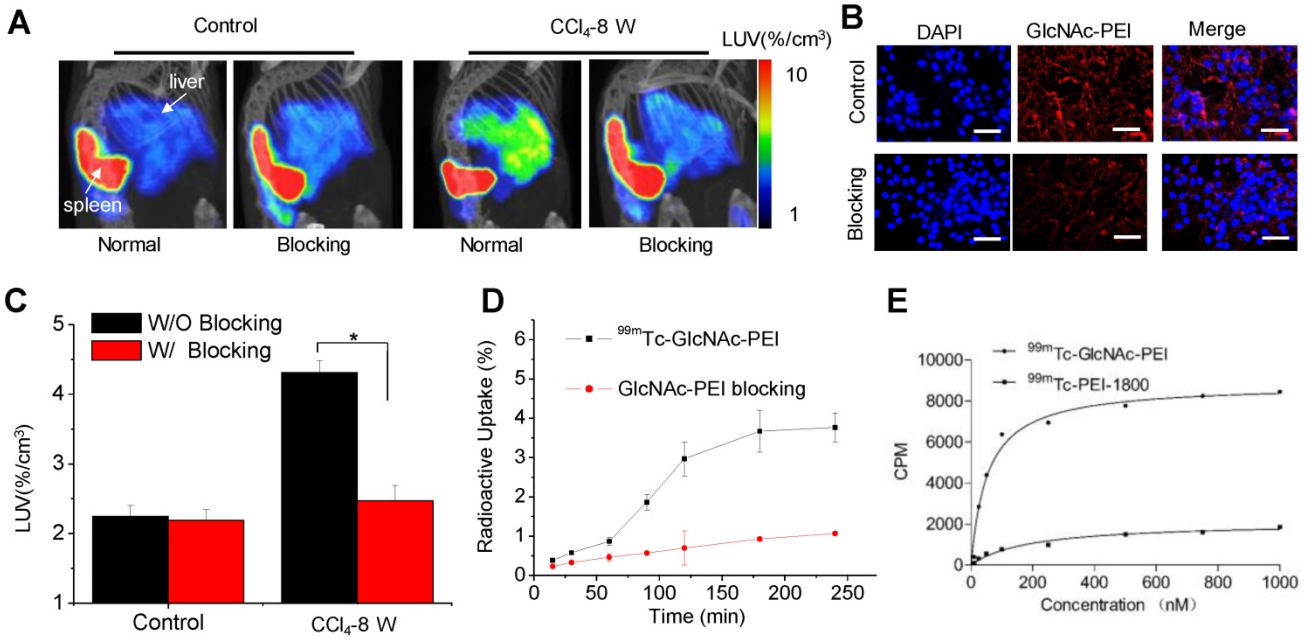

Fig. 4. Blocking studies of ^{99m}Tc-GlcNAc-PEI in fibrotic mice. (A) SPECT/CT imaging of fibrotic mice at 30 min after the intravenous injection of ^{99m}Tc-GlcNAc-PEI (18.5 MBq) with or without GlcNAc-PEI for blocking. Images were adjusted using the same scale for all animals. (B) Cell uptake of GlcNAc-PEI-Cy5.5 in the fibrotic liver tissue. Blue: DAPI; Red: GlcNAc-PEI-Cy5.5. Scale bar: 50 μm. (C) Hepatic uptake of ^{99m}Tc-GlcNAc-PEI derived from SPECT imaging by drawing the ROI of the whole liver. (D) Competitive binding assay of ^{99m}Tc-GlcNAc-PEI with or without the presence of excess GlcNAc-PEI in HSCs separated from the liver of fibrotic mice. (E) Saturation binding assay of ^{99m}Tc-GlcNAc-PEI with desmin protein.

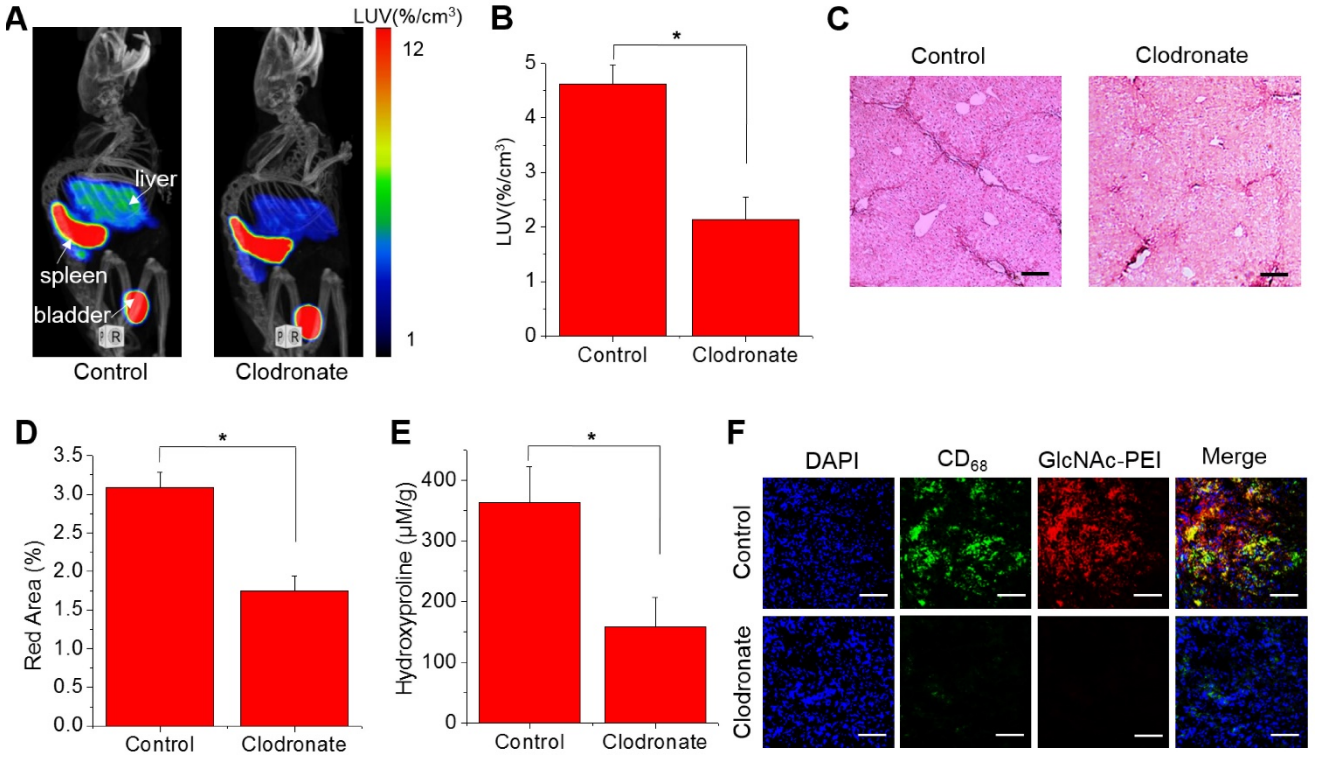

Fig. 5. ^{99m}Tc-GlcNAc-PEI SPECT/CT imaging of liver fibrosis mice with clodronate liposome treatment. (A) ^{99m}Tc-GlcNAc-PEI SPECT/CT imaging of fibrotic mice with clodronate liposome treatment. (B) Hepatic uptake of ^{99m}Tc-GlcNAc-PEI by drawing the ROI of the whole liver. (C) Representative images of Sirius Red staining after clodronate liposome treatment. Scale bar: 200 μm. (D) Quantization of the red area of Sirius Red staining after treatment with clodronate liposome. (E) Hydroxyproline level in the liver of CCl_4-induced mice after treatment with clodronate liposomes. (F) Immunofluorescence staining of fibrotic liver tissue after treatment with clodronate liposome. Blue: DAPI; green: anti-CD_{68} staining FITC; Red: GlcNAc-PEI-Cy5.5. Scale bar: 200 μm. $^{*}P$ <0.05 and $^{**}P$ <0.01.

Interestingly, a very high spleen uptake was found in both SPECT imaging and the biodistribution of ^{99m}Tc-GlcNAc-PEI that could not be blocked by the co-injection of cold compound. In the SPECT imaging study, the spleen uptake values in the control and blocking groups were 28.46 ± 2.54%/cc vs 25.40 ± 1.58%/cc (P = 0.15, Fig. 4A), respectively, indicating non-specific uptake. Although the exact mechanism is not clear, it may be related to the lymphocyte activation in the spleen based on the reports that GlcNAc modification of protein may play an important role in lymphocyte activation[21].

There were several other radiotracers reported to image liver fibrosis in mouse or rat models. Asialoglycoprotein (ASGP) receptor-targeting radiotracers have been used to assess liver fibrosis by quantifying hepatic function after liver injury[22,23]. Although these ASGP-R-targeting radiotracers were useful in detecting advanced fibrosis and cirrhosis, they might be not very sensitive in the detection of early and mild fibrosis because they assess liver fibrosis by measuring hepatic function, which did not directly reflect the degree of fibrosis. Furthermore, a series of RGD peptide-based radiotracers had been developed for SPECT imaging by targeting active HSCs[24,25]. Regarding HSC-target radiotracers, they could reliably reflect the degree of fibrosis and detect early fibrosis. However, the high uptake of those radiotracers in the kidney influenced the quality of liver images and was not good for the quantitation of hepatic uptake. Compared with these previously reported radiotracers, we developed a new agent of ^{99m}Tc-GlcNAc-PEI by specifically targeting desmin and vimentin to activate HSCs, reflecting liver fibrosis directly and could be used to detect liver fibrosis as early as 4 weeks after CCl_4 treatment. Furthermore, there was a very high binding affinity and lower kidney uptake of ^{99m}Tc-GlcNAc-PEI ensuring the high quality of SPECT/CT image which might be beneficial to diagnose early and mild hepatic fibrosis in the clinical setting.

In addition to monitoring the progression of liver fibrosis induced by CCl_4 treatment, we also investigated whether ^{99m}Tc-GlcNAc-PEI SPECT/CT imaging could be used to monitor the response of drug treatment. Although removing the causative agent is thought to be the most effective intervention in the treatment of liver fibrosis[26,27], it is difficult to remove the causative agent of liver diseases (for example, HCV and fatty liver). As reported by Wynn et al.[28], macrophages produce profibrotic mediators that directly activate fibroblasts, including transforming growth factor-β1 (TGF-β1) and platelet-derived growth factor (PDGF), and control the ECM turnover by regulating the balance of various matrix metalloproteinases (MMPs) and tissue inhibitors of matrix metalloproteinases (TIMPs). Considering that clodronate could deplete macrophages in the liver[29], we used clodronate liposomes to treat liver fibrosis. The results of our study suggested that treatment with clodronate can degrade collagen fibers and reduce liver fibrosis. In the meantime, hepatic uptake of ^{99m}Tc-GlcNAc-PEI was obviously decreased in the fibrotic mice after treatment with clodronate. Therefore, ^{99m}Tc-GlcNAc-PEI SPECT imaging could be a useful method in monitoring the response to treatment in live fibrosis.

Conclusion

Here, we demonstrated that the non-invasive method based on SPECT/CT imaging with ^{99m}Tc-GlcNAc-PEI can be used to monitor fibrosis progression and evaluated the efficacy of anti-fibrotic drugs in a mouse model. SPECT/CT imaging with ^{99m}Tc-GlcNAc-PEI may be a potential strategy for noninvasive diagnosis of hepatic fibrosis in the clinic.

Materials and methods

Synthesis of GlcNAc-PEI

GlcNAc-PEI was synthesized according to a previous report with slight modifications[30]. Briefly, chitobiose (0.1 g) was dissolved in 20% aqueous methanol and was mixed with 0. 285 g of iodine. Next, 1 mol/L of potassium hydroxide solution was slowly dropped into the mixture until the iodine color completely disappeared. Thereafter, the solution was concentrated in vacuo to produce crude chitobionic acid. The 25 mol% chitobionic acid solution was then reacted with PEI-1800 (Sigma-Aldrich, St Louis, MO, USA) using water-soluble carbodiimide [1-ethyl-3-3(-dimethylaminopropyl)carbodiimide hydrochloride (EDC) (Sigma-Aldrich, St Louis, MO, USA) as a coupling agent, under stirring at room temperature. After stirring at room temperature for 24 h, the solution was dialyzed for 48 h using a dialysis membrane with a cutoff of 2500 Da.

Radiolabeling and stability studies

Briefly, 100 μg/100 μL of GlcNAc-PEI and 20 μL of $SnCl_2$ (2 mg/mL in 0.1 M HCl) were mixed in a vial. Next, 185~370 MBq of freshly $Na^{99m}TcO_4$ obtained from Zhongshan Hospital affiliated with Xiamen University was added to the mixture. The reaction mixture was then allowed to incubate at room temperature for 30 min to obtain the resulting radiotracer ^{99m}Tc-GlcNAc-PEI. The labeling efficiency of ^{99m}Tc-GlcNAc-PEI was determined by instant thin-layer chromatography (ITLC). The

chromatography analyses were performed on ITLC silica gel strips (Pall Life Sciences, Ann Arbor, MI, USA) with acid-citrate-dextrose buffer (0.068 M citrate, 0.074 M dextrose, pH 5.0) as a mobile phase. The stability of the radiotracer was tested in the same way after incubation in saline or mice serum at 37 °C for 4 h. Next, all the strips were detected using a Mini-Scan radio-TLC Scanner (BioScan, Poway, CA, USA).

Liver fibrosis mouse model and antifibrotic therapy

CCl_4 (Sigma Aldrich, St Louis, MO, USA) was used to produce hepatic fibrosis in mice. Briefly, CCl_4 was dissolved in olive oil (1:4), and 5 mL/kg body weight of CCl_4 solution was injected intraperitoneally into 6-week-old female C57BL/6 mice twice a week for 4 or 8 weeks. Control group was administered with same doses of olive oil (n = 5 for each group). All the mice were obtained from the Laboratory Animal Center of Xiamen University. All animal care and experiments were approved by Xiamen University's animal care and use committee.

Clodronate liposome (Clodrosome, Brentwood, TN, USA) was used for the treatment of liver fibrosis. The 8 weeks CCl_4-induced fibrotic mice (n = 5) were administered with 5 mL/kg clodronate liposome by tail-vein injection once a week for 2 weeks. The control group was administered the same doses of PBS liposome (n = 5). All the mice were imaged one week after the last injection to avoid the acute effects of CCl_4.

SPECT/CT Imaging

SPECT/CT imaging was performed using a pinhole collimator microSPECT/CT scanner (Mediso, Budapest, Hungary) and standard animal scan procedures. Static SPECT/CT imaging of fibrotic (CCl_4-4 W and CCl_4-8 W) and control mice (n = 4 for each group) were performed at 30 min after tail-vein injection of 18.5 MBq of ^{99m}Tc-GlcNAc-PEI. The animals were anesthetized by 2% isoflurane during SPECT imaging. Blocking experiments were performed with the co-injection of an excess dose of GlcNAc-PEI (500 μg). The LUV derived from SPECT/CT imaging was used to assess the stage of liver fibrosis. The LUV was calculated by dividing the radioactivity of the whole liver by the total inject radioactivity and whole liver volume as previously described[31].

Biodistribution

To determine the binding of ^{99m}Tc-GlcNAc-PEI in liver tissues of fibrotic mice, we divided the mice were divided into 3 groups (control, and CCl_4-4 W and CCl_4-8 W fibrotic mice, n = 3 for each group). Each mouse was injected with 37 kBq/100 μL of ^{99m}Tc-GlcNAc-PEI via the tail vein. The mice were sacrificed under ether narcotization 30 min after injection. Organs and tissues of interest were collected and weighed. The radioactivity of the organs and tissues was measured using a gamma counter (WIZARD 2480, Perkin-Elmer, Downers Grove, IL, USA). The percentage of the injected dose per gram (%ID/g) of organs and tissues was calculated.

Immunofluorescent assay

After imaging, the livers of the control and fibrotic mice were frozen in CRYO GLUE tissue embedding medium (SLEE medical GmbH, Mainz, GER) and were stored in a −80 °C freezer. Subsequently, the specimens were cut into 7-μm slices. The liver tissues were fixed using 4% paraformaldehyde for 10 min. The liver tissues were blocked with 1% bovine serum albumin (BSA) for 30 min, incubated with monoclonal desmin antibodies (1:150 dilution, Abcam, Shanghai, CN), vimentin antibodies (1:100 dilution, Abcam) or α-SMA antibodies (1:100 dilution, Abcam) at 4 °C overnight, and then incubated with FITC-conjugated secondary antibodies (1:200 dilution, Sigma-Aldrich, St Louis, MO, USA) and GlcNAc-PEI-Cy5.5 for 30 min at room temperature. The cell nuclei were stained with 4,6-diamidino-2-phenylindole (DAPI) solution for 10 min. Images were captured by a confocal microscope (FV1200, Olympus, Aizu, JPN).

Radioactive competitive binding assay

Mouse HSCs were isolated from fibrotic mice as previously reported[32]. Briefly, mouse HSCs were harvested and seeded in 24-well plates at 10^5 cells per well. Twenty-four hours later, the cells were washed twice with binding buffer (phosphate buffer solution with 0.5% BSA) and for 1 h at 37 °C with 1.85 kBq of ^{99m}Tc-GlcNAc-PEI. Blocking group was performed with co-incubation with 500 nM GlcNAc-PEI. After incubation, the cells were washed twice with binding buffer and solubilized with 1 N NaOH. Radioactivity of the cell was measured with a gamma counter (WIZARD 2480, Perkin-Elmer, Waltham, MA, USA).

Saturation binding assay

Briefly, 0.5 mL of 2 μM recombinant human desmin protein (ARP, Waltham, MA, USA) or vimentin protein from bovine lens (ARP) was incubated for 1 h on ice with increasing concentrations of ^{99m}Tc-GlcNAc-PEI or ^{99m}Tc-PEI-1800 from 0 to 1,000 nmol/L. After incubation, unbound ligand was removed using an Amicon® Ultra-4 10K centrifugal filter (Merck Millipore, Co. Cork, IRL) by centrifugation for 10 min at 1,000 g, and radioactivity

was measured in a γ-counter. The data were analyzed using GraphPad Prism 5.

Tissue analysis

Liver tissue was embedded in paraffin, after fixation with paraformaldehyde. Subsequently, the specimens were cut into 5-μm-thick sections and were stained with Sirius Red according to standard procedures. Hydroxyproline in liver tissue was quantified by HPLC analysis according to previous reports[33].

Statistical analysis

Quantitative data are presented with error bars as the means ± SD. Statistical differences among groups were determined by Student's t-test. The Pearson correlation coefficient was computed to measure the linear relationship between two quantitative variables, and significance was evaluated by two-tailed test. Differences were considered significant when *P* values were less than 0.05.

Abbreviations

ECM: extracellular matrix; HSC: hepatic stellate cells; GlcNAc: N-acetylglucosamine; SPECT: single photon emission computed tomography; PEI: polyethylenimine; CCl_4: carbon tetrachloride; LUV: Liver uptake value; ROI: region of interest; a-SMA: α smooth muscle actin; RCP: radiochemical purity; ASGP: asialoglycoprotein; TGF-β1: transforming growth factor-β1; PDGF: platelet-derived growth factor; MMPs: matrix metalloproteinases; TIMPs: tissue inhibitors of matrix metalloproteinases; EDC: [1-ethyl-3-3(-dimethylaminopropyl)carbodiimide hydrochloride; ITLC: instant thin-layer chromatography; %ID/g: injected dose per gram; BSA: bovine serum albumin; DAPI: 4,6-diamidino-2-phenylindole.

Supplementary Material

Supplementary figures and methods.
http://www.thno.org/v08p1340s1.pdf

Acknowledgments

This study was financially supported by the National Key Basic Research Program of China (2014CB744503), National Natural Science Foundation of China (21271030, 81471707) and Scientific Research Foundation of State Key Laboratory of Molecular Vaccinology and Molecular Diagnostics (2016ZY002).

Competing Interests

The authors have declared that no competing interest exists.

References

1. Friedman SL. Mechanisms of hepatic fibrogenesis. Gastroenterology. 2008; 134: 1655-1669.
2. Bataller R, Brenner DA. Liver fibrosis. J Clin Invest. 2005; 115: 209-218.
3. Guido M, Rugge M, Chemello L, et al. Liver stellate cells in chronic viral hepatitis: the effect of interferon therapy. J Hepatol. 1996; 24: 301-307.
4. Friedman SL. Liver fibrosis – from bench to bedside. J Hepatol. 2003; 38: 38-53.
5. Reeves HL, Burt AD, Wood SJ, et al. Hepatic stellate cell activation occurs in the absence of hepatitis in alcoholic liver disease and correlates with the severity of steatosis. J Hepatol. 1996; 25: 677-683.
6. Rockey DC, Caldwell SH, Goodman ZD, et al. American Association for the Study of Liver D. Liver biopsy. Hepatology. 2009; 49: 1017-1044.
7. Manning DS, Afdhal NH. Diagnosis and quantitation of fibrosis. Gastroenterology. 2008; 134(6): 1670-1681.
8. Polasek M, Fuchs BC, Uppal R, et al. Molecular MR imaging of liver fibrosis: a feasibility study using rat and mouse models. J Hepatol. 2012; 57: 549-555.
9. Friedrich-Rust M, Ong MF, Martens S, et al. Performance of transient elastography for the staging of liver fibrosis: a meta-analysis. Gastroenterology. 2008; 134: 960-974.
10. Poynard T, Vergniol J, Ngo Y, et al. Staging chronic hepatitis C in seven categories using fibrosis biomarker (FibroTest) and transient elastography (FibroScan(R)). J Hepatol. 2014; 60: 706-714.
11. Ezetimibe for the treatment of nonalcoholic steatohepatitis: assessment by novel magnetic resonance imaging and magnetic resonance elastography in a randomized trial (MOZART trial). Hepatology. 2015; 61(4): 1239-1250
12. Cohen E, Afdhal NH. Ultrasound-based hepatic elastography: origins, limitations, and applications. J Clin Gastroenterol. 2010; 44: 637-645.
13. Ise H, Kobayashi S, Goto M, et al. Vimentin and desmin possess GlcNAc-binding lectin-like properties on cell surfaces. Glycobiology. 2010; 20: 843-864.
14. Komura K, Ise H, Akaike T. Dynamic behaviors of vimentin induced by interaction with GlcNAc molecules. Glycobiology. 2012; 22: 1741-1759.
15. Niki T, Pekny M, Hellemans K, et al. Class VI intermediate filament protein nestin is induced during activation of rat hepatic stellate cells. Hepatology. 1999; 29: 520–527.
16. Kim SJ, Ise H, Goto M, et al. Interactions of vimentin- or desmin-expressing liver cells with N-acetylglucosamine-bearing polymers. Biomaterials. 2012; 33: 2154-2164.
17. Puche JE, Saiman Y, Friedman SL. Hepatic stellate cells and liver fibrosis. Arch Pathol Lab Med. 2013; 3: 1473.
18. Kim SJ, Ise H, Kim E, et al. Imaging and therapy of liver fibrosis using bioreducible polyethylenimine/siRNA complexes conjugated with N-acetylglucosamine as a targeting moiety. Biomaterials. 2013; 34: 6504-6514.
19. Yoshida M, Shiraishi S, Sakaguchi F, et al. A quantitative index measured on (9)(9)mTc GSA SPECT/CT 3D fused images to evaluate severe fibrosis in patients with chronic liver disease. Jpn J Radiol. 2012; 30: 435-441.
20. Popov Y, Schuppan D. Targeting liver fibrosis: Strategies for development and validation of antifibrotic therapies. Hepatology. 2009; 50: 1294-1306.
21. Kearse KP, Hart GW. Lymphocyte activation induces rapid changes in nuclear and cytoplasmic glycoproteins. Proc Natl Acad Sci U S A. 1991; 88: 1701-1705.
22. Sorensen M, Mikkelsen KS, Frisch K, et al. Regional metabolic liver function measured in patients with cirrhosis by 2-[(1)(8)F]fluoro-2-deoxy-D-galactose PET/CT. J Hepatol. 2013; 58: 1119-1124.
23. Taniguchi M, Okizaki A, Watanabe K, et al. Hepatic clearance measured with (99m)Tc-GSA single-photon emission computed tomography to estimate liver fibrosis. World J Gastroenterol. 2014; 20: 16714-16720.
24. Li F, Song Z, Li Q, et al. Molecular imaging of hepatic stellate cell activity by visualization of hepatic integrin alphavbeta3 expression with SPECT in rat. Hepatology. 2011; 54: 1020-1030.
25. Guo Z, Gao M, Zhang D, et al. Simultaneous SPECT imaging of multi-targets to assist in identifying hepatic lesions. Sci Rep. 2016; 6: 28812.
26. Pares A, Caballeria J, Bruguera M, et al. Histological course of alcoholic hepatitis. Influence of abstinence, sex and extent of hepatic damage. J Hepatol. 1986; 2: 33-42.
27. Arthur MJP. Reversibility of liver fibrosis and cirrhosis following treatment for hepatitis C. Gastroenterology. 2002; 122: 1525-1528.
28. Wynn TA, Barron L. Macrophages: master regulators of inflammation and fibrosis. Semin Liver Dis. 2010; 30: 245-257.

29. Navarro LA, Wree A, Povero D, et al. Arginase 2 deficiency results in spontaneous steatohepatitis: a novel link between innate immune activation and hepatic de novo lipogenesis. J Hepatol. 2015; 62: 412-420.
30. Kim SJ, Ise H, Goto M, et al. Gene delivery system based on highly specific recognition of surface-vimentin with N-acetylglucosamine immobilized polyethylenimine. Biomaterials. 2011; 32: 3471-3480.
31. Zhang D, Guo Z, Zhang P, et al. Simplified quantification method for in vivo SPECT/CT imaging of asialoglycoprotein receptor with (99m)Tc-p(VLA-co-VNI) to assess and stage hepatic fibrosis in mice. Sci Rep. 2016; 6: 25377.
32. Miyahara T, Schrum L, Rippe R, et al. Peroxisome proliferator-activated receptors and hepatic stellate cell activation. J Biol Chem. 2000; 275: 35715-35722.
33. Hutson PR, Crawford ME, Sorkness RL. Liquid chromatographic determination of hydroxyproline in tissue samples. J Chromatogr B. 2003; 791: 427-430.